Uncertainties in eddy covariance flux measurements assessed from CH_4 and N_2O observations

P.S. Kroon[a,b]
A. Hensen[a]
H.J.J. Jonker[b]
H.G. Ouwersloot[a,b]
A.T. Vermeulen[a]
F.C. Bosveld[c]

[a]Energy research Centre of the Netherlands (ECN), Petten, The Netherlands
[b]Delft University of Technology (TU Delft), Delft, The Netherlands
[c]Royal Dutch Meteorological Institute (KNMI), De Bilt, The Netherlands

Published in Agricultural and Forest Meteorology 150 (2010) 806–816

ECN-W--10-030 March 2010

Agricultural and Forest Meteorology 150 (2010) 806–816

Contents lists available at ScienceDirect

Agricultural and Forest Meteorology

journal homepage: www.elsevier.com/locate/agrformet

Uncertainties in eddy covariance flux measurements assessed from CH_4 and N_2O observations

P.S. Kroon [a,b,*], A. Hensen [a], H.J.J. Jonker [b], H.G. Ouwersloot [a,b], A.T. Vermeulen [a], F.C. Bosveld [c]

[a] Energy research Centre of the Netherlands (ECN), Department of Air Quality and Climate Change, Westerduinweg 3, 1755 LE Petten, The Netherlands
[b] Delft University of Technology (TU Delft), Department of Multi-Scale Physics, Research Group Clouds, Climate and Air Quality, Lorentzweg 1, 2628 CJ Delft, The Netherlands
[c] Royal Dutch Meteorological Institute (KNMI), Section Atmospheric Research, Wilhelminalaan 10, 3732 GK De Bilt, The Netherlands

ARTICLE INFO

Article history:
Received 15 January 2009
Received in revised form 9 July 2009
Accepted 31 August 2009

Keywords:
CH_4 fluxes
Correction
N_2O fluxes
Uncertainty

ABSTRACT

The uncertainty in eddy covariance (EC) flux measurements is assessed for CH_4 and N_2O using data measured at a dairy farm site in the Netherlands in 2006 and 2007. An overview is given of the contributing uncertainties and their magnitude. The relative and absolute uncertainty of a 30 min EC flux are estimated for CH_4 and N_2O using $N = 2185$ EC fluxes. The average absolute uncertainty and its standard deviation are 500 ± 400 ng C m^{-2} s^{-1} for CH_4 and 100 ± 100 ng N m^{-2} s^{-1} for N_2O. The corresponding relative uncertainties have 95% confidence interval ranging from 20% to 300% for CH_4 and from 30% to 1800% for N_2O. The large relative uncertainties correspond to relatively small EC fluxes. The uncertainties are mainly caused by the uncertainty due to one-point sampling which contributes on average more than 90% to the total uncertainty. The other 10% includes the uncertainty in the correction algorithm for the systematic errors. The uncertainty in a daily and monthly averaged EC flux are estimated for several flux magnitude ranges. The daily and monthly average uncertainty are smaller than 25% and 10% for CH_4 and smaller than 50% and 10% for N_2O, respectively, based on fluxes larger than 100 ng C m^{-2} s^{-1} and 15 ng N m^{-2} s^{-1}.

1. Introduction

The greenhouse gasses methane (CH_4) and nitrous oxide (N_2O) play an important role in global warming, with global warming potentials 23 and 296 times greater than CO_2 for a 100 years time horizon (IPCC, 2001). Agricultural soils are major sources of both gasses (IPCC, 2006). To determine integrated emission estimates on a hectare scale that also have continuous coverage in time, high frequency micrometeorological methods are often used.

A limited number of eddy covariance (EC) measurements of CH_4 and N_2O has been published using lead salt tunable diode laser (TDL) spectrometers and quantum cascade laser (QCL) spectrometers (e.g. Smith et al., 1994; Wienhold et al., 1994; Laville et al., 1999; Hargreaves et al., 2001; Werle and Kormann, 2001; Eugster et al., 2007; Kroon et al., 2007; Neftel et al., 2007). In these studies, the CH_4 and N_2O exchanges are given over different time periods ranging from a week to several years. The averaged emission rates are given together with their standard deviations. However, the standard deviation of the average is mainly an indication of the temporal variability of the CH_4 and N_2O exchanges. Moncrieff et al. (1996) suggested that it might be a good convention to represent the mean flux together with its uncertainty when results from studies employing EC flux systems are represented. However, the uncertainties in the averaged emission rates are rarely indicated in the present literature. These uncertainties are composed of several uncertainties related to atmospheric conditions, measurement method and data analysis method. For example, there are uncertainties due to limited precision of the measurements, frequency response correction and calibration correction.

In this paper, we will give an overview of the uncertainties in EC flux measurements of CH_4 and N_2O. This overview consists of a physical description, an estimation tool and a quantitative derivation for each uncertainty that is partly based on literature. The focus is on the uncertainty of a single 30 min EC flux measurement. Knowing the uncertainty at such a small time scale is important to quantify, since single EC flux values are used among others for model parameterizations that aim at resolving the diurnal cycle. In addition, we will derive the uncertainties over longer time scales using the 30 min EC uncertainty. All uncertainties are estimated after applying the corrections for systematic errors, e.g. density effects and frequency response losses. These corrections have not always been applied in previous studies.

* Corresponding author at: Energy research Centre of the Netherlands (ECN), Department of Air Quality and Climate Change, Westerduinweg 3, 1755 LE Petten, The Netherlands. Tel.: +31 224 564062; fax: +31 224 568488.
E-mail address: p.kroon@ecn.nl (P.S. Kroon).

0168-1923/$ – see front matter © 2009 Elsevier B.V. All rights reserved.
doi:10.1016/j.agrformet.2009.08.008

Therefore, we will emphasize the importance of applying the corrections here. All examples are based on EC flux data measured at a dairy farm site in the Netherlands in 2006 and 2007. Consequently, the given uncertainties will be partly specific for our measurement set-up; however, most uncertainties are generally applicable to other EC set-ups.

2. Experimental site and climatic conditions

We have performed the measurements at an intensively managed dairy farm. This farm is located at Oukoop near the town Reeuwijk in the Netherlands (52°02′11″N, 4°46′49″E). The surrounding area of the measurement location has soil consisting of a clayey peat or peaty clay layer of about 0.25 m on about 12 m eutrophic peat deposits. Rye grass (*Lolium perenne*) is the most dominant grass species with often co-dominant rough bluegrass (*Poa trivialis*) and clover species constitute less than 1% of the vegetation (Veenendaal et al., 2007). The site is located in a polder where the water level is managed. The mean elevation of the polder is between 1.6 and 1.8 m below sea level (ASL). About 21% of the area is open water (Nol et al., 2008) and the ditch water level is being kept at −2.39 in winter and −2.31 m ASL in summer. The climate is temperate and wet with an average temperature of 11.1 °C in 2006 and 2007. The total precipitation was 767 and 1087 mm in 2006 and 2007, respectively (based on KNMI data measured at Cabauw, the Netherlands). Manure and fertilizer were applied about five times a year from February to September, and there were about four harvest events. Annual manure and artificial fertilizer were about 55 $m^3\ ha^{-1}$ (253 kg N ha^{-1}) and 370 kg ha^{-1} (100 kg N ha^{-1}) in 2006, and 57 $m^3\ ha^{-1}$ (262 kg N ha^{-1}) and 350 kg ha^{-1} (95 kg N ha^{-1}) in 2007.

3. Instrumentation and methodology

3.1. Instrumentation

We used two separate masts since the measurements were performed by two research groups. Both masts of 3 m height were positioned in the middle of the field about 3 m from each other. The terrain around the masts was flat and free of obstruction for at least 600 m in all directions, except for a container in which the QCL spectrometer was placed. The container of 2 m × 2 m × 2 m was located at about 20 m northeast from the two masts to avoid flow distortion. The first mast was equipped with instruments for latent heat fluxes and the second mast for CH_4 and N_2O fluxes. Latent heat fluxes were measured by University of Wageningen with an EC system consisting of a Campbell SCAT C3 sonic anemometer (Campbell Scientific, Logan, Utah, USA) and a Licor 7500 open path Infrared gas analyzer (LICOR Lincoln, NE, USA), see Veenendaal et al. (2007) for more information about this set-up. Wind speed, air temperature, CH_4 and N_2O concentrations were measured with a system consisting of a three-dimensional sonic anemometer (model R3, Gill Instruments, Lymington, UK) and a QCL spectrometer (model QCL-TILDAS-76, Aerodyne Research Inc., Billerica MA, USA). The R3 sonic was replaced for a WMPRO (Gill Instruments, Lymington, UK) on 25 October 2007.

The air inlet tube was located at 0.15 m from the sonic anemometer heart. We used a 25 m polyethylene inlet tube with a diameter of 0.25 inch. We controlled the flow and cell pressure with a needle valve at the inlet of the multi-pass cell. A vacuum pump (TriScoll 600, Varian Inc., USA) with a maximum volume flow rate of 400 l min^{-1} was located downstream of the multi-pass cell. The flow in the tube was turbulent with Reynolds number and flow rate of about 4000 and 9.2 m s^{-1}. In order to dry the air before analyzing, we installed a membrane drier (Perma Pure) at 13 September 2007. We kept the cell pressure constant before and after installing the membrane drier so that no change occurred in the high frequency attenuation. After that date, corrections for density fluctuations due to water vapor flux did not need to be applied anymore. The correction due to sensible heat flux was omitted since a constant temperature and pressure in the sampling cell were maintained. The temperature and pressure in the cell were continuously measured and corrections were made automatically for small fluctuations using TDL-Wintel software.

The QCL used the 1270 and 1271 cm^{-1} absorption lines for CH_4 and N_2O, respectively, and required liquid nitrogen cooling for maximum sensitivity in the used wavelength region. We calibrated the QCL spectrometer at least once a week for correcting differences from absolute concentration values using mixtures in N_2/O_2 of 1700 and 5100 ppb and 300 and 610 ppb for CH_4 and N_2O, respectively (Scott speciality gasses, the Netherlands).

The sonic anemometer and the QCL spectrometer data were logged using the RS232 output and we processed the data using a program developed at ECN, following the procedures of McMillen (1988). A more detailed explanation of this measurement set-up is given in Kroon et al. (2007).

3.2. Methodology

3.2.1. EC flux determination including corrections

The EC flux is one of the terms needed for the quantification of the net ecosystem exchange. The expression for the net ecosystem exchange of CH_4 (F_{CH_4}) and N_2O (F_{N_2O}) is derived by the tracer conservation equation (e.g. Aubinet et al., 2000). Assuming horizontal homogeneity and a flat terrain within the averaging time of 30 min, the net ecosystem exchange F_{wc} consists of two contributions, the storage change term St_c and the eddy covariance flux term EC_{wc}, and is given by

$$F_{wc} = \underbrace{\frac{\bar{c}_i - \bar{c}_{i-1}}{T_{av}} h}_{St_c} + \underbrace{\overline{w'c'}|_{z=h}}_{EC_{wc}} \quad (1)$$

where h is the measurement height in m, i the flux number, T_{av} the averaging time in s, w the vertical wind velocity in m s^{-1} and c the gas concentration in ppb. We calculate the storage change term using the average values of CH_4 and N_2O at 3 m height over each 30 min period.

We derive the eddy covariance flux term in several steps. First, we determine the time average of w and c using a running mean filter (e.g. Aubinet et al., 2000; Lee et al., 2004). A running mean filter is a practical solution to filter laser drift contributions which occurred due to interference fringes in the optical system and small movements of the fringes due to temperature and pressure effects. The laser drift contributions behave like additional noise on the signal which can lead to a higher detection limit. We set the running mean filter constant to the time scale on which laser drift starts, which has been derived using an Allan Variance analyses (Kroon et al., 2007). This filter could cause an under- or overestimation of the flux due to filtering of large eddies contributions. Second, we calculate the covariances using a running mean filter constant τ_f of 120 s and an averaging time of 30 min. The covariances are corrected for tilt error using the natural wind coordinate system (e.g. McMillen, 1988; Lee et al., 2004). Furthermore, the exact delay time is determined using circular correlation (Kroon et al., 2007). The exact delay time is dependent on the flow rate in the tube which is related to the performance of the pump and the resistance of the inlet filters. However, the delay time cannot always be defined very well using the correlation method, most notably for small N_2O fluxes. Therefore, we use an adapted strategy for the delay determination. We assume that the delay time of N_2O is equal to the delay time of

CH_4 since both gasses are inert and no wall effects at the inlet system are expected. Consequently, the delay time of CH_4 is determined for each 30 min time slot and the delay time is set during each day to the 30 min delay time which occurs most often for CH_4 during that day. The day by day adaptation seems to be appropriate since no diurnal pattern is found in the delay time. The delay time is only linked to the degradation of the filters and the flow.

The measured EC flux EC_{wc}^{meas} is not equal to the real EC flux EC_{wc} since systematic errors occur in the measurements. Therefore, we apply some corrections before the final EC flux EC_{wc} is derived. The EC flux is given by

$$EC_{wc} = \chi_{cal}\chi_{res}EC_{wc}^{meas} + \chi_{cal}\chi_{Webb} \quad (2)$$

with χ_{res} the frequency response correction, χ_{Webb} the Webb-correction and χ_{cal} the calibration correction. A frequency response correction is applied since not all fluctuations in the frequency range, where transport takes place, are represented by the sensors. Contributions at low frequencies are not well included because of the running mean filter, and contributions at high frequencies are not well measured due to sensor separation, path averaging of the sonic anemometer, attenuation effects in the tube and the limited response time of the QCL. The contributions of all frequencies to the EC flux are described using the co-spectral density function $C_{wc}(f)$ which is related to the covariance as (e.g. Stull, 1988; Kaimal and Finnigan, 1994; Aubinet et al., 2000)

$$\overline{w'c'} = \int_0^\infty C_{wc}(f)df \quad (3)$$

in which f represents the natural frequency in Hz. Low and high frequency filtering cause that the measured eddy flux EC_{wc}^{meas} is given by (e.g. Aubinet et al., 2000)

$$EC_{wc}^{meas} = \int_0^\infty T(f)C_{wc}(f)df \quad (4)$$

where $T(f)$ denotes the net transfer function. The net transfer function consists of a low and high frequency transfer function that are multiplied in frequency space. We use the (empirical) normalized Kaimal co-spectrum $E_{wc}(z/L, U, f)$ for deriving the correction term χ_{res} for low and high frequency response losses (Kaimal et al., 1972). Moore (1986) determined expressions for the normalized co-spectrum during stable ($z/L > 0$) and unstable atmospheric ($z/L < 0$) conditions based on the Kaimal co-spectrum where L represents the Monin–Obukhov length scale. The response correction factor χ_{res} is calculated by (e.g. Aubinet et al., 2000)

$$\chi_{res} = \frac{\int_0^\infty E_{wc}(f)df}{\int_0^\infty T_{low}(f)T_{high}(f)E_{wc}(f)df} \quad (5)$$

where $T_{low}(f)$ and $T_{high}(f)$ denote the high and low frequency response transfer function, respectively. Moore (1986) provided expressions for both transfer functions. The low frequency transfer function is given by

$$T_{low}(f) = \frac{(2\pi f\tau_f)^2}{1 + (2\pi f\tau_f)^2} \quad (6)$$

with τ_f the running mean time in s, assuming that this transfer function is only dependent on the running mean filter, and the high frequency transfer function is described by

$$T_{high}(f) = T_s(f)T_r(f) \quad (7)$$

for this particular measurement set-up (Kroon et al., 2009), where $T_s(f)$ and $T_r(f)$ denote the transfer functions for sensor separation and limited response time, respectively. For illustration, we plot an average measured co-spectrum for CH_4 and N_2O

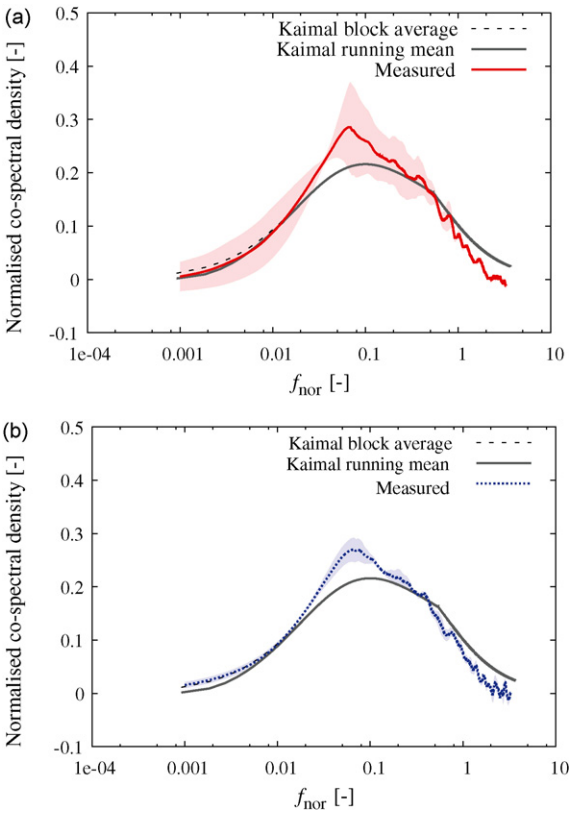

Fig. 1. Spectral behavior of an average of three 30 min EC fluxes during unstable conditions with $U = 1.83\ m\ s^{-1}$ and $z/L = -0.37$ based on block average together with the Kaimal co-spectrum for a block average and a 120 s running mean filter for CH_4 (a) and N_2O (b).

with average mean wind velocity $U = 1.83\ m\ s^{-1}$ and average stability parameter $z/L = -0.37$ (Fig. 1). These co-spectra are derived using three normalized co-spectra based on a block average of 30 min. We show the average co-spectra together with its uncertainty, the Kaimal block average and 120 s running mean co-spectra. The measured co-spectrum and Kaimal co-spectrum are in good agreement at low frequencies for both gasses. The differences in contributions are within the uncertainty range for CH_4 and just outside the uncertainty range for N_2O. However, the measured and empirical Kaimal co-spectra differ at the high frequencies.

Both frequency losses are dependent on the mean wind velocity and the stability. Low frequency losses are larger during unstable conditions and low mean wind velocities and high frequency losses during stable conditions and high mean wind velocities. Consequently, the investigated situation favored low frequency losses; however, still the high frequency losses are much more prominent than the low frequency losses for this specific measurement set-up.

The second correction that we apply is the Webb-correction χ_{Webb}. This correction is made since the assumption $\bar{w} \cdot \bar{c} = 0$ in the vertical constituent flux

$$EC_{wc} = \chi_{cal}\chi_{res}\overline{w'c'} + \chi_{cal}\bar{w}\bar{c} \quad (8)$$

is not correct in general considering that turbulent motion consists of ascending and descending parcels, which have different densities caused by the vertical gradients of potential temperature and specific humidity. The vertical velocities of up and down going parcels are different in order to maintain the mass balance. Consequently, there is a mean vertical wind velocity which differs

from zero. Therefore, the EC flux is corrected before the total vertical flux is obtained. The engineering form of the Webb-correction is used, which is given by (Webb et al., 1980)

$$\tilde{\chi}_{\mathrm{Webb}} = \left(\frac{\overline{\rho_c}}{\overline{\rho_a}}\right)(0.649 \times 10^{-6}\lambda E + 3.358 \times 10^{-6} H) \quad (9)$$

where $\tilde{\chi}_{\mathrm{Webb}}$ is in kg m^{-2} s^{-1}, λE and H are the sensible and latent heat flux in W m^{-2}, ρ_c and ρ_a are the gas and air density in kg m^{-3}, respectively. We only partly apply the Webb-correction since a constant temperature and pressure were maintained in the sampling cell. Therefore, we only perform the Webb-correction for the influence of water vapor fluctuations. In addition, we installed a membrane drier (Perma Pure) in order to dry the air before analyzing at 13 September 2007, in consequence, the Webb-correction was not longer necessary after that date. We derive the Webb-correction term using the latent heat flux data of the University of Wageningen. The Webb-correction based on this open path EC system probably overestimates the correction because damping of concentration and water vapor fluctuations has already taken place in the 25 m inlet tube of the closed EC system. Since we derived the EC fluxes in ppb m s^{-1}, the Webb-correction χ_{Webb} is also needed in ppb m s^{-1} which is derived using the ideal gas law

$$\chi_{\mathrm{Webb}} = \tilde{\chi}_{\mathrm{Webb}} 10^{12}\left(\frac{RT_{\mathrm{air}}}{P_{\mathrm{air}}M_c}\right) \quad (10)$$

where χ_{Webb} is equal to $\overline{w.c}$ in equation 8, with R = 8.3145 J mol^{-1} K^{-1} the gas constant, T_{air} the air temperature, P_{air} the air pressure and M_c the molar mass which is 16 and 44 g mol^{-1} for CH_4 and N_2O, respectively.

Finally, we use a two-point calibration factor based on weekly calibrations for correcting the absolute concentration values. The calibration correction factor χ_{cal} determined at a certain calibration session is described by

$$\chi_{\mathrm{cal}} = \frac{S_H - S_L}{M_H - M_L} \quad (11)$$

where S_H and S_L denote the high and low CH_4 and N_2O standard concentration values in ppb coming from a gas cylinder and M_H and M_L denote the high and low measured concentration values in ppb. The EC fluxes between two calibration sessions are corrected by the average calibration factor of both calibration sessions.

Thus, the net ecosystem exchange F_{wc} of CH_4 and N_2O is composed of a storage change and an EC flux term (Eq. (1)). The EC flux over 30 min is calculated using Eq. (2). Next, the F_{wc} data is flagged using the in-stationary test of Foken and Wichura (1996) and the fetch is checked by a footprint model based on the Kormann–Meixner method (Kormann and Meixner, 2001). By means of this, we reject the 30 min value when the flag is larger than 2 and when less than 70% of the flux came from the dairy farm site.

3.2.2. Uncertainty determination

As this study addresses the uncertainty in EC flux measurements of CH_4 and N_2O, we derive an expression for the uncertainty of a single EC flux measurement. The uncertainty consists of several uncertainties either linked to the correction processes of systematic errors or linked to processes for which no correction could be made. Some of these uncertainties have been discussed in the literature (e.g. Businger, 1986; Moncrieff et al., 1996). To indicate clearly all uncertainties, we give an overview of them in Table 1. All these uncertainties are random and the degree of randomness is indicated in this Table. Random uncertainties have the property that they decrease with increasing data set size according to $1/\sqrt{N}$ where N denotes the number of independent realizations. For example, for the uncertainty in the precision of the concentration measurement, N indicates the number of measurement points, which is equal to 36,000 for a single 30 min EC flux measurement and for the uncertainty in the systematic frequency response correction factor; N indicates the number of 30 min EC flux measurements. We assume that the uncertainties with degree of randomness per measurement point are negligible in comparison with all other uncertainties. In addition, we do not discuss the uncertainties due to the alignment of the sonic anemometer,

Table 1
An overview of uncertainties in EC flux measurements, and their degree of randomness which reveals the random uncertainty due to random errors and the random uncertainty in the correction factors of the systematic errors.

Uncertainty symbol	Description	Degree of randomness	References
u_{prc}[a]	Precision of concentration measurement	Per measurement point	Allan (1966); Werle and Kormann (2001); Nelson et al. (2004); Kroon et al. (2007); Hendriks et al. (2008)
u_{drc}[a]	Drift in concentration measurement	Per measurement point	Allan (1966); Werle and Kormann (2001); Nelson et al. (2004); Kroon et al. (2007)
u_{prw}[a]	Precision of vertical wind velocity measurement	Per measurement point	Manual sonic anemometers
u_{op}	One-point sampling of turbulence	Per 30 min EC flux	Businger (1986); Moncrieff et al. (1996)
u_{low}	Inadequate length of sampling	Per 30 min EC flux	Van den Hurk (1996); Moncrieff et al. (1996)
	Low frequency filtering technique (running mean filter)	Per 30 min EC flux	Aubinet et al. (2000)
u_{high}	Limited response time	Per 30 min EC flux	Businger (1986); Van den Hurk (1996); Moncrieff et al. (1996)
	Low sampling rate	Per 30 min EC flux	Bosveld and Beljaars (2001)
	Inadequate height above the surface	Per 30 min EC flux	Businger (1986); Van den Hurk (1996); Moncrieff et al. (1996)
	Tube attenuation	Per 30 min EC flux	Van den Hurk (1996)
u_{Webb}	Webb-correction	Per 30 min EC flux	Webb et al. (1980); Businger (1986); Moncrieff et al. (1996)
u_{cal}	Consistent over- or underestimation of fluxes by calibrations	Per calibration period	Moncrieff et al. (1996)
u_{al}[b]	Alignment sonic anemometer	Per 30 min EC flux	McMillen (1988); Lee et al. (2004)
u_{delay}[a]	Delay time determination	Per day	This study
u_{fp}[b]	Footprint (inadequate fetch)	Per 30 min EC flux	Businger (1986); Moncrieff et al. (1996)
u_{nst}[b]	Non-stationarity	Per 30 min EC flux	Businger (1986); Van den Hurk (1996); Moncrieff et al. (1996)
u_{ad}[b]	Advection	Per 30 min EC flux	Businger (1986)
u_{en}[b]	Entrainment	Per 30 min EC flux	Businger (1986)
u_{dis}[b]	Flow distortion	Per 30 min EC flux	Businger (1986); Moncrieff et al. (1996)

[a] Uncertainty is negligible.
[b] Uncertainty is not covered in this study.

footprint, non-stationarity, advection and flow distortion in this study.

We estimate the uncertainty in a 30 min EC flux EC_{wc} (Eq. (2)) by combining the uncertainties using (e.g. Taylor, 1982)

$$u(EC_{wc}) = \sqrt{\left(u_{cal}\frac{\partial EC_{wc}}{\partial \chi_{cal}}\right)^2 + \left(u(\chi_{res})\frac{\partial EC_{wc}}{\partial \chi_{res}}\right)^2 + \left(u(EC_{wc}^{meas})\frac{\partial EC_{wc}}{\partial EC_{wc}^{meas}}\right)^2 + \left(u_{Webb}\frac{\partial EC_{wc}}{\partial \chi_{Webb}}\right)^2} \quad (12)$$

where we assume no correlation between the uncertainties. After partial differentiation this leads to

$$u(EC_{wc}) = \sqrt{\left(u_{cal}(\chi_{res}EC_{wc}^{meas} + \chi_{Webb})\right)^2 + \left(u(\chi_{res})\chi_{cal}EC_{wc}^{meas}\right)^2 + \left(u(EC_{wc}^{meas})\chi_{cal}\chi_{res}\right)^2 + \left(u_{Webb}\chi_{cal}\right)^2} \quad (13)$$

Thus, the uncertainty $u(EC_{wc})$ consists of four uncertainties, namely the random uncertainty in $w'c'$, $u(EC_{wc}^{meas})$, the frequency response correction uncertainty $u(\chi_{res})$, the Webb-correction uncertainty u_{Webb} and the calibration correction uncertainty u_{cal}. The uncertainty $u(EC_{wc}^{meas})$ is dominated by the uncertainty due to one-point sampling since we assume that the uncertainty contributions of the measurement precision of the vertical wind velocity and concentration are negligible. Businger (1986) derived the following estimate for the one-point uncertainty

$$u_{op} = \sqrt{\frac{2}{M}}\sigma_{w'c'} \quad (14)$$

where $\sigma_{w'c'}$ represents the standard deviation in the quantity $w'c'$, i.e. $\sqrt{\overline{(w'c')^2} - \left(\overline{w'c'}\right)^2}$ and where M denotes the number of *independent* measurements of $w'c'$. Expression (14) is based on the common idea that the uncertainty in the mean value can be reduced by increasing the number of realizations. But note that M cannot be made larger by simply increasing the sampling rate with which $w'c'$ are measured, since this will not produce more independent measurements; after all, the high sampling rate measurements are highly correlated. Rather, the number of independent measurements M is determined by the largest time scale of the turbulent process (large eddy turnover time) in relation to the entire measurement period T_{av}. Businger estimated the turbulence time scale at $10z/U$, making M approximately equal to $T_{av}U/10z$. The one-point uncertainty is then $u_{op} = \sqrt{20z/T_{av}U}\sigma_{w'c'}$. Following Businger (1986), we rewrite this expression by introducing the non-dimensional factor

$$\varphi = \left|\frac{\overline{(w'c')^2} - \left(\overline{w'c'}\right)^2}{\left(\overline{w'c'}\right)^2}\right| \quad (15)$$

which embodies interesting information on the statistical distribution of the flux values. Then

$$u_{op} = aEC_{wc}^{meas} = \sqrt{\frac{20z\varphi}{T_{av}U}}\overline{w'c'} \quad (16)$$

where a denotes the relative uncertainty in the measured EC flux. This uncertainty even occurs when the assumption of stationarity and horizontal homogeneity are fulfilled for the turbulent atmospheric flow.

The second uncertainty is the uncertainty in the frequency response correction χ_{res} (Eq. (5)). Evaluating the integral, one obtains an expression for χ_{res} which formally depends on the following parameters

$$\chi_{res} = \chi_{res}(U, z/L, \tau_f, \tau_r, s) \quad (17)$$

where U and z/L originated from the Kaimal co-spectrum, and τ_f, τ_r and s from the transfer functions. We ignore the uncertainties in the determination of U and z/L and no uncertainty is associated with the running mean value of $\tau_f = 120$ s. In principle $u(\chi_{res}) = \sqrt{((\partial\chi_{res}/\partial\tau_r)u(\tau_r))^2 + ((\partial\chi_{res}/\partial s)u(s))^2}$, but since we have no analytical expression for the integral, we estimate the uncertainty by numerically evaluating the integral for two values of response time and sensor separation time, i.e. for τ_r and s, and for $\tau_r + \Delta\tau_r$ and $s + \Delta s$ which leads to

$$u(\chi_{res}) = \left|\chi_{res}(\tau_r + \Delta\tau_r, s + \Delta s) - \chi_{res}(\tau_r, s)\right|. \quad (18)$$

Next, the uncertainty in the Webb-correction for water vapor fluctuations (Eqs. (9) and (10)) u_{Webb} is estimated by

$$u_{Webb} = \sqrt{\sum_{i=1}\left(u(x_i)\frac{\partial\chi_{Webb}}{\partial x_i}\right)^2} \quad (19)$$

where x_i are $\bar{\rho}_c$, $\bar{\rho}_a$, T_{air}, P_{air} and λE. We assume that the uncertainties in $\bar{\rho}_c$, $\bar{\rho}_a$, T_{air} and P_{air} are negligible in comparison to the uncertainty in the latent heat flux λE. The uncertainty in the Webb-correction is then approximately equal to

$$u_{Webb} = \sqrt{\left(u(\lambda E)\left(0.649 \times 10^{-6}\left(\frac{\bar{\rho}_c}{\bar{\rho}_a}\right)\left(\frac{RT_{air}}{P_{air}M_c}\right)10^{12}\right)\right)^2}. \quad (20)$$

The last uncertainty is the calibration correction uncertainty $u_{cal.}$ We determine this uncertainty over each calibration period. Thus, the degree of randomness is equal to the amount of calibration periods. Each calibration period is only based on two calibration sessions (Eq. (11)). Therefore, we cannot use the classical method for statistical uncertainties for the quantification of this uncertainty. We set the uncertainty u_{cal} to

$$u_{cal} = \left|\frac{\chi_{cal}[i] - \chi_{cal}[i-1]}{2}\right| \quad (21)$$

where we divide by 2 since the used χ_{cal} is within χ_{cal} $[i]$ and χ_{cal} $[i-1]$.

Next to these four uncertainties, there are also two other uncertainties in a single EC flux, namely the delay time uncertainty and the uncertainty in the spectral shape at the low frequencies. Both are not taken into account in Eq. (13). We do not include the delay time determination uncertainty because of two reasons. First, we assume that this uncertainty is negligible for 30 min EC fluxes for which the CH_4 fluxes are larger than the detection limit of 41 ng C m^{-2} s^{-1} (Kroon et al., 2007). At this peat area, the CH_4 fluxes are mainly larger than the detection limit. For example: the CH_4 flux and its standard deviation were found to be 512 ± 385 ng C m^{-2} s^{-1} over the fertilizing event of 2006 (Kroon et al., 2007). But, the detection limit could be larger since it is dependent on the alignment of the system. However, when CH_4 fluxes are smaller than the detection limit, the uncertainty due to the delay time determination has probably already been included in the uncertainty due to one-point sampling. We will show this in the next section. In spite of no additional contribution to the overall uncertainty, we still recommend comparing the delay times of CH_4 with the delay times of CO_2 when CO_2 is measured with the same instrumental set-up since the delay time can be much easier obtained for CO_2 than for CH_4 because of much larger flux values.

In addition, we do not include the uncertainty in the spectral shape at the low frequencies since it is not directly included into one of the correction algorithms. However, it is still interesting to address this uncertainty. We focus on the uncertainty at low frequency contributions since this uncertainty is larger than the uncertainty at high frequency contributions among others due to less independent realizations. Consequently, the spectral shape uncertainty is larger during unstable than stable conditions. To get

a rough indication, we estimate this uncertainty using an Ogive analysis, which is given by Lee et al. (2004) and Kroon et al. (2007)

$$\mathrm{Og}_{wc}(f_m) = \sum_{i=m}^{(n_s-1)/2} |E_{wc}(f_i)| \quad (22)$$

where

$$f_i = \frac{i}{(n_s-1)\Delta t}; \quad m = 1, 2, \ldots, \left[\frac{n_s-1}{2}\right].$$

In this case, the Ogives are determined by integrating the absolute normalized co-spectrum derived by block averaging starting from the high frequencies. The absolute co-spectra are calculated over one hour. The total contribution at 120 s (8.3×10^{-3} Hz) is compared for several Kaimal co-spectra with several measured co-spectra. A rough indication of the uncertainty in the measured co-spectra is then derived by

$$u_{\text{co-spectra}} = \left| \frac{\overline{\mathrm{Og}_{wc}(8.3\times10^{-3})_{\text{Kaim}}} - \overline{\mathrm{Og}_{wc}(8.3\times10^{-3})_{\text{meas}}}}{2} \right|. \quad (23)$$

In summary, the uncertainty in a single EC flux measurement is given by Eq. (13) in which four uncertainties are given, the random uncertainty in $w'c'$, $u(\mathrm{EC}_{wc}^{\text{meas}})$, which is dominated by the one-point uncertainty u_{op}, the frequency response correction uncertainty $u(\chi_{\text{res}})$, the Webb-correction uncertainty u_{Webb} and the calibration correction uncertainty u_{cal}. The uncertainties u_{op}, $u(\chi_{\text{res}})$, u_{Webb} and u_{cal} are described by Eqs. (16), (18), (20) and (21), respectively.

4. Estimation of the EC flux uncertainty

4.1. Estimation of the uncertainties

We estimate the uncertainties $u(\mathrm{EC}_{wc}^{\text{meas}})$, $u(\chi_{\text{res}})$, u_{Webb} and u_{cal} in this section where the uncertainty $u(\mathrm{EC}_{wc}^{\text{meas}})$ is assumed to be equal to the one-point uncertainty u_{op}. We determine the uncertainty u_{op} in three steps, first we estimate φ using Eq. (15), then the relative uncertainty a with Eq. (16) and finally we determine u_{op} with Eq. (16). Wyngaard (1973) plotted φ for sensible heat flux as function of z/L. He found a value of $\varphi \approx 10$ using the Kansas data for near neutral conditions. Businger (1986) assumed that the same value could be used for scalar fluxes. However, to our knowledge the value of φ has not been determined for CH_4 and N_2O. Therefore, we check whether $\varphi \approx 10$ is a reasonable estimate for CH_4 and N_2O fluxes using the published data set in Kroon et al. (2007).

We select $N = 375$ 30 min EC flux values which satisfy the criteria, CH_4 and N_2O fluxes larger than 500 ng C m^{-2} s^{-1} and 50 ng N m^{-2} s^{-1}, respectively. In general, we find that the distribution of φ resembles a lognormal distribution. Consequently, the geometric mean and standard deviation are calculated. The geometric mean and standard deviation are 38 and 2 for CH_4, and 524 and 7 for N_2O, respectively. The 95% confidence interval ranges from 8 to 179 for CH_4 and from 11 to 26×10^3 for N_2O. Thus, φ is significantly larger than 10 for both gasses, probably caused by the fact that the CH_4 and N_2O fluxes are relatively small and closer to the detection limit than the sensible heat fluxes used in the study of Wyngaard (1973). In addition, the φ value for N_2O is much larger than the φ value for CH_4. As an example, we plot φ as function of z/L for which we sort 375 EC fluxes by z/L and classified them in 25 bins of 15 measurements each (Fig. 2). We show the geometric mean of φ over each bin as function of the arithmetic mean of z/L.

To investigate whether the relatively large φ values are caused by the EC flux magnitude, we determine φ as function of the flux magnitude. We derive φ for $N = 2325$ 30 min EC flux values for both gasses. Then, we sort the EC fluxes by magnitude and classify them in 31 bins of 75 measurements each. Next, the geometric average and uncertainty are calculated over each bin. In Fig. 2, we show φ as function of the flux magnitude there, it can be seen that φ decreases with increasing flux magnitude. The relatively large uncertainty at small EC flux values is probably caused by relatively large noise contributions since the fluxes are smaller or just larger than the detection limit. Because of that, we assume that the uncertainty due to the delay time determination has already been included in the one-point uncertainty. The geometric average of φ is 23 and 57 for the last bin with average EC fluxes $\mathrm{EC}_{wc}^{\text{meas}}$ of 1021 ng C m^{-2} s^{-1} and 132 ng N m^{-2} s^{-1} for CH_4 and N_2O, respectively. These φ values are closer to the factor of 10 shown in Businger (1986) than φ based on all the selected 375 EC fluxes.

Next, we estimate the relative uncertainty a due to a one-point measurement using φ and Eq. (16). The same 31 bins with 75 measurements each are used and we calculate the geometric average of the uncertainty a and its uncertainty as function of the flux magnitude. This leads to an average a range from 51% to 391% for CH_4 and from 71% to 809% for N_2O (Fig. 3), where the smallest a corresponds to the largest EC flux. The indications of 51% and 71% are in the same range of the indicated uncertainties of some other EC flux studies (Businger, 1986). The corresponding 95% confidence intervals of the last bins range from 16% to 156% for CH_4 and from 18% to 273% for N_2O. As indicated in Eq. (16), we expect that the relative uncertainty a decreases with increasing wind velocity. However in this study, we have not found a significant effect of increasing wind velocity which is probably due to the relatively large uncertainties in φ.

To investigate the behavior of φ in more detail, we derive an analytical expression for φ for the case where w' and c' are given by a zero-mean joint-Gaussian stochastic process (see Appendix A). We obtain the following expression for φ

$$\varphi = \frac{1}{\rho_{wc}^2} + 1 \quad (24)$$

with ρ_{wc} the correlation coefficient. Since $|\rho_{wc}| < 1$, this result shows that φ is bounded from below (the minimal value is $\varphi = 2$ at $\rho_{wc} = 1$), but not from above as φ diverges for $\rho_{wc} \to 0$. This leads us to conclude that there is no good justification for setting φ to a "universal" value, because even for an elementary Gaussian process φ can take any value larger than 2. Consequently, it appears to be much wiser to stay close to the definition and treat the one-point sampling uncertainty as an absolute contribution.

Therefore, we calculate the absolute one-point measurement uncertainty u_{op}. As an example: we plot several EC fluxes and their uncertainties due to one-point averaging in Fig. 3. It is shown that the temporal variation of the flux exceeds the uncertainty in EC flux measurements. However, the magnitude of the estimated uncertainty u_{op} is very significant compared to the magnitude of the EC fluxes. This makes clear that further evaluation of this issue is important. Large Eddy Simulations (LES) are a good candidate to further address the issue of the uncertainty in EC flux measurements due to the one-point averaging principle.

The second uncertainty in the total EC flux uncertainty (Eq. (13)) is the frequency response correction uncertainty $u(\chi_{\text{res}})$ which is given by Eq. (18). Thus, we investigate the effect of a small change in response time τ_r and in sensor separation s. We set $\tau_r + \Delta\tau_r$ and $s + \Delta s$ to 0.11 s and 0.18 m, respectively, and τ_r and s to 0.08 s and 0.15 m. The data is split into two velocity ranges, one from 2 to 4 m s^{-1} ($N = 361$) and one with velocities larger than 4 m s^{-1} ($N = 259$). For each range, the EC fluxes are sorted by stability z/L and binned in several groups with 25 measurements each. Then, we determine the average and standard deviation over each bin for the uncertainty $u(\chi_{\text{res}})$ and the stability z/L and they are plotted for both velocity ranges in Fig. 4. It is shown that the high frequency uncertainty is dependent on the stability and the

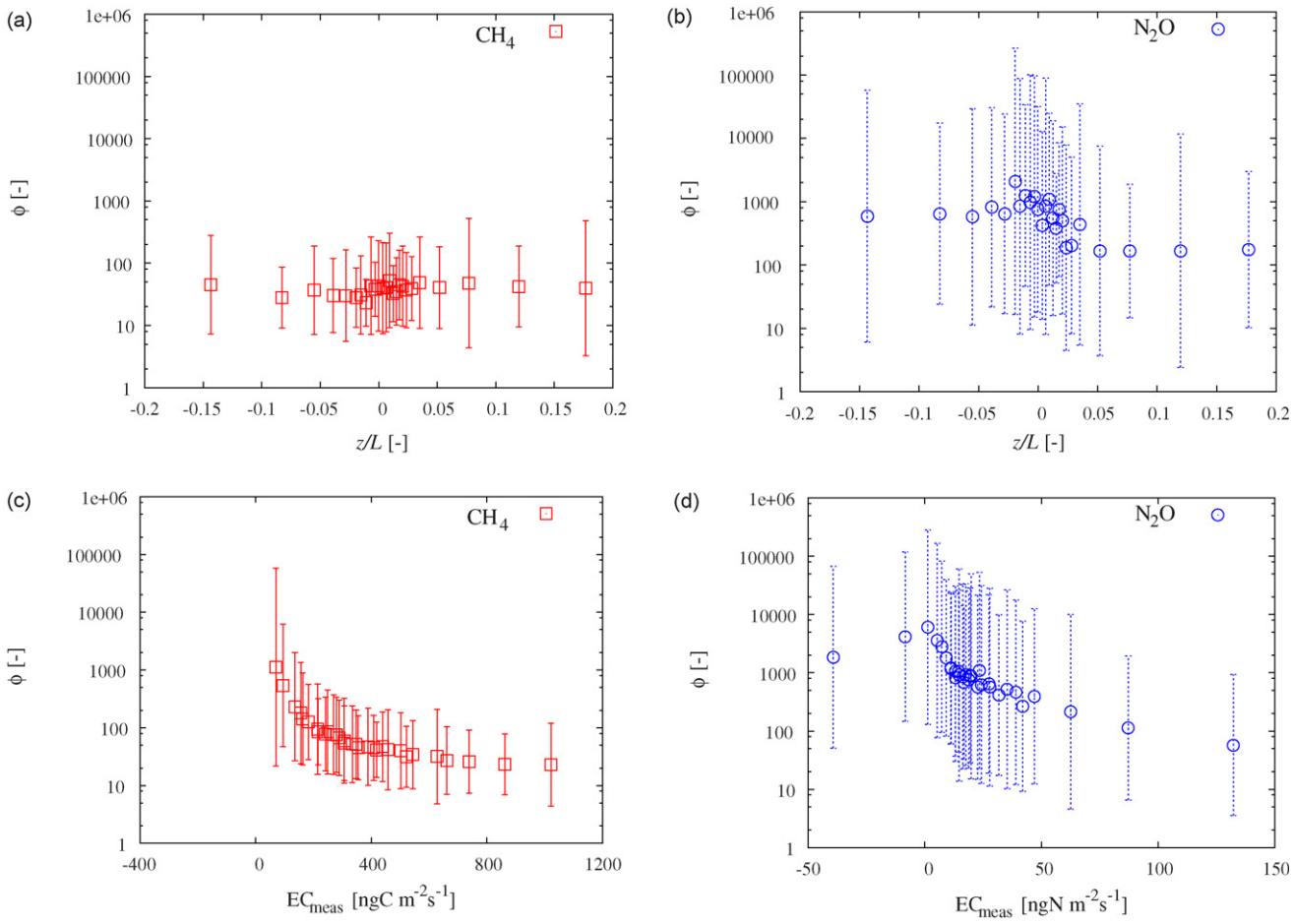

Fig. 2. Values of $\varphi = \left(\overline{(w'c')^2} - (\overline{w'c'})^2\right)/(\overline{w'c'})^2$ using the published dataset in Kroon et al. (2007). The geometric mean and 95% confidence interval of φ for 25 bins with 15 measurements each are given as function of the stability parameter z/L for CH_4 (a) and N_2O (b) where only fluxes larger than 500 ng C m^{-2} s^{-1} and 50 ng N m^{-2} s^{-1} are taken into account for CH_4 and N_2O, respectively. In addition, the geometric mean and 95% confidence interval of φ for 31 bins with 75 measurements each is shown as function of the EC flux magnitude for CH_4 (c) and N_2O (d).

mean wind velocity. In this study, we use the maximum estimated uncertainty in the stability range z/L from −1 to 1 which is 0.08.

The third uncertainty in the total EC flux uncertainty is the Webb-correction uncertainty u_{Webb}. This correction is dependent on the latent and sensible heat flux (Eqs. (9) and (10)). The Webb-correction is only applied for water vapor fluctuations since the QCL automatically corrects for temperature fluctuations. The effect of the Webb-correction is very dependent on the flux magnitude of CH_4 and N_2O. The relative effect of the Webb-correction can be much larger than 100%. The Webb-correction is most important for small fluxes and therefore more prominent for N_2O than for CH_4. This correction can turn small negative fluxes into small positive fluxes. In consequence, the uncertainty u_{Webb} depends on the uncertainty of the latent heat flux (Eq. (20)). The random uncertainty of the latent heat flux is estimated using Eq. (16) assuming that the one-point measurement uncertainty is dominant. We set the measurement height at 3 m, the averaging time at 30 min and φ at 10. The random uncertainty ranges then from 18% to 58% for a mean wind velocity range from 1 to 10 m s^{-1}. In addition, we assume a systematic uncertainty of 20%.

Furthermore, we estimate the last uncertainty in the total EC flux uncertainty, the calibration uncertainty u_{cal}. First, we determine the average calibration factor of CH_4 and N_2O and standard deviations over $N = 37$ time periods, which are 1.42 ± 0.13 and 1.31 ± 0.11 for CH_4 and N_2O, respectively. Then the corresponding uncertainty u_{cal} and its standard deviations are calculated using Eq. (21), which lead to 0.13 ± 0.10 and 0.11 ± 0.10 for CH_4 and N_2O, respectively. We recommend performing calibrations at smaller time intervals to decrease this uncertainty.

Finally, we give just a rough indication of the uncertainty in the spectral shape at low frequencies. We select $N = 65$ EC fluxes for CH_4 and N_2O with CH_4 fluxes larger than 500 ng C m^{-2} s^{-1} and N_2O fluxes larger than 100 ng N m^{-2} s^{-1}. Then, we determine the average and standard deviation of Og_{wc} $(8.3 \times 10^{-3})_{Kaim}$ and Og_{wc} $(8.3 \times 10^{-3})_{meas}$. The average and standard deviation are 95% ± 5%, 86% ± 8% and 81% ± 14% for the Kaimal co-spectrum, the measured CH_4 co-spectrum and measured N_2O co-spectrum. Thus, the estimated uncertainty is about 5% and 7% for CH_4 and N_2O, respectively, derived using Eq. (23). In addition, the eddy contribution of times scales larger than 30 min are found to be less than 2% for all three cases. Consequently, the difference can probably partly be explained by possible drift contributions at time scales larger than 120 s. However, this difference can also still partly be caused by high frequency response losses. In this study, we use a running mean filter of 120 s to avoid drift contributions and we have already corrected for high frequency response losses. However, we still recommend checking the importance of a running mean filter when EC flux measurements are performed by QCL or TDL spectrometry. In addition, the low frequency range of the co-spectrum is still under discussion (e.g. Jonker et al., 1999; De Roode et al., 2004) especially for unstable conditions, and should be investigated in more detail.

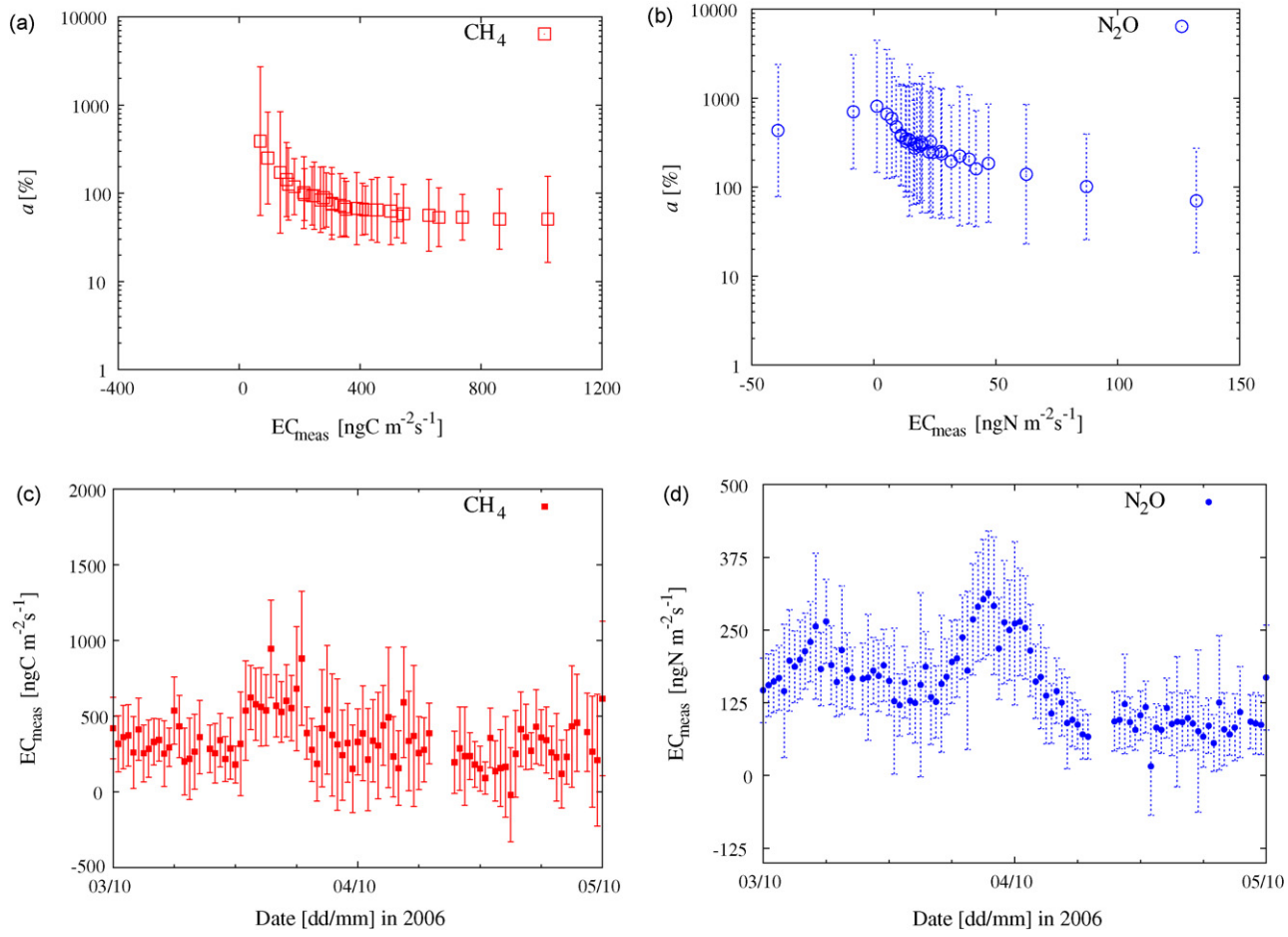

Fig. 3. The relative and absolute uncertainty due to one-point measurement given by $u_{op} = a\mathrm{EC}_{wc}^{meas} = \sqrt{20z\varphi/T_{av}Uw'c}$ using the published dataset in Kroon et al. (2007). The geometric mean and 95% confidence interval of the relative uncertainty a for 31 bins with 75 measurements each are shown as function of the EC flux for CH_4 (a) and N_2O (b). EC fluxes and their absolute uncertainty due to one-point sampling are given for CH_4 (c) and N_2O (d) over the period 3 to 5 October 2006.

4.2. Total EC flux uncertainty

We determine the 30 min EC flux uncertainty using Eq. (13) for $N = 2185$ fluxes in the period from August 2006 to November 2006 for which data is available for all required parameters. This equation consists of several terms which are derived in the following way. The uncertainty $u(\mathrm{EC}_{wc}^{meas})$ and the variable EC_{wc}^{meas} are determined using equation 16 and 4, respectively, for each 30 min period. Then, we use $u(\chi_{res}) = 0.08$ and we calculate χ_{res} using Eq. (5) for each 30 min EC flux where $T_{low}(f) = 1$. In addition, the uncertainty u_{Webb} is determined using Eq. (20) with $u(\lambda E) = \lambda E\sqrt{(0.2)^2 + \left(\sqrt{200z/T_{av}U}\right)^2}$ and the correction factor χ_{Webb} using Eq. (10). Finally, the calibration factor χ_{cal} and its uncertainty u_{cal} are determined over each calibration period using Eqs. (11) and (21).

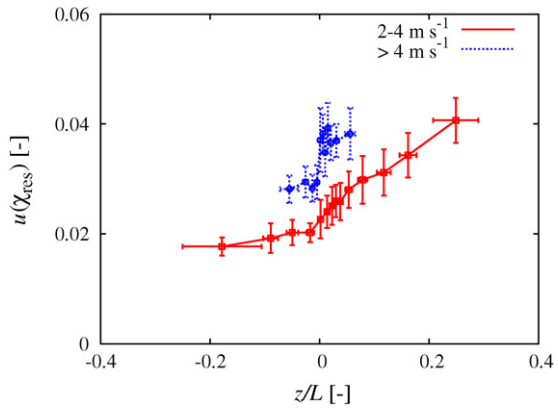

Fig. 4. Indication of the uncertainty in the frequency response correction factor given by $u(\chi_{res}) = |\chi_{res}(\tau_r + \Delta\tau_r, s + \Delta s) - \chi_{res}(\tau_r, s)|$ with $\tau_r + \Delta\tau_r = 0.11$ s, $s + \Delta s = 0.18$ m, $\tau_r = 0.08$ s and $s = 0.15$ m, as function of the stability z/L for two velocity regimes. Each data point represents the average z/L and relative high frequency uncertainty value of 25 measurements with their standard deviation.

After all these steps, the absolute and relative uncertainty are estimated of a 30 min EC flux (Fig. 5). The average absolute uncertainty and its standard deviation are 453 ± 380 ng C m^{-2} s^{-1} for CH_4 and 117 ± 101 ng N m^{-2} s^{-1} for N_2O. The relative uncertainty distribution resembles a lognormal distribution. The geometric average and standard deviation are 80% and 186% for CH_4, and 225% and 283% for N_2O, respectively. The 95% confidence intervals range from 23% to 279% for CH_4 and from 28% to 1806% for N_2O.

The total uncertainty consists of four terms (Eq. (13)). The third term $\left(u(\mathrm{EC}_{wc}^{meas})\chi_{cal}\chi_{res}\right)^2$ is most important and contributes on average 93% and 96% to the total uncertainty in net ecosystem exchange F_{CH_4} and F_{N_2O}, respectively. The uncertainty in EC_{wc}^{meas} is approximately equal to the absolute one-point uncertainty u_{op}. This uncertainty is just slightly dependent on the EC flux magnitude.

Thus, the uncertainty in a 30 min EC flux can be even larger than the flux itself. However, more accurate estimates of F_{wc} can be obtained when longer time spans than 30 min are used since all

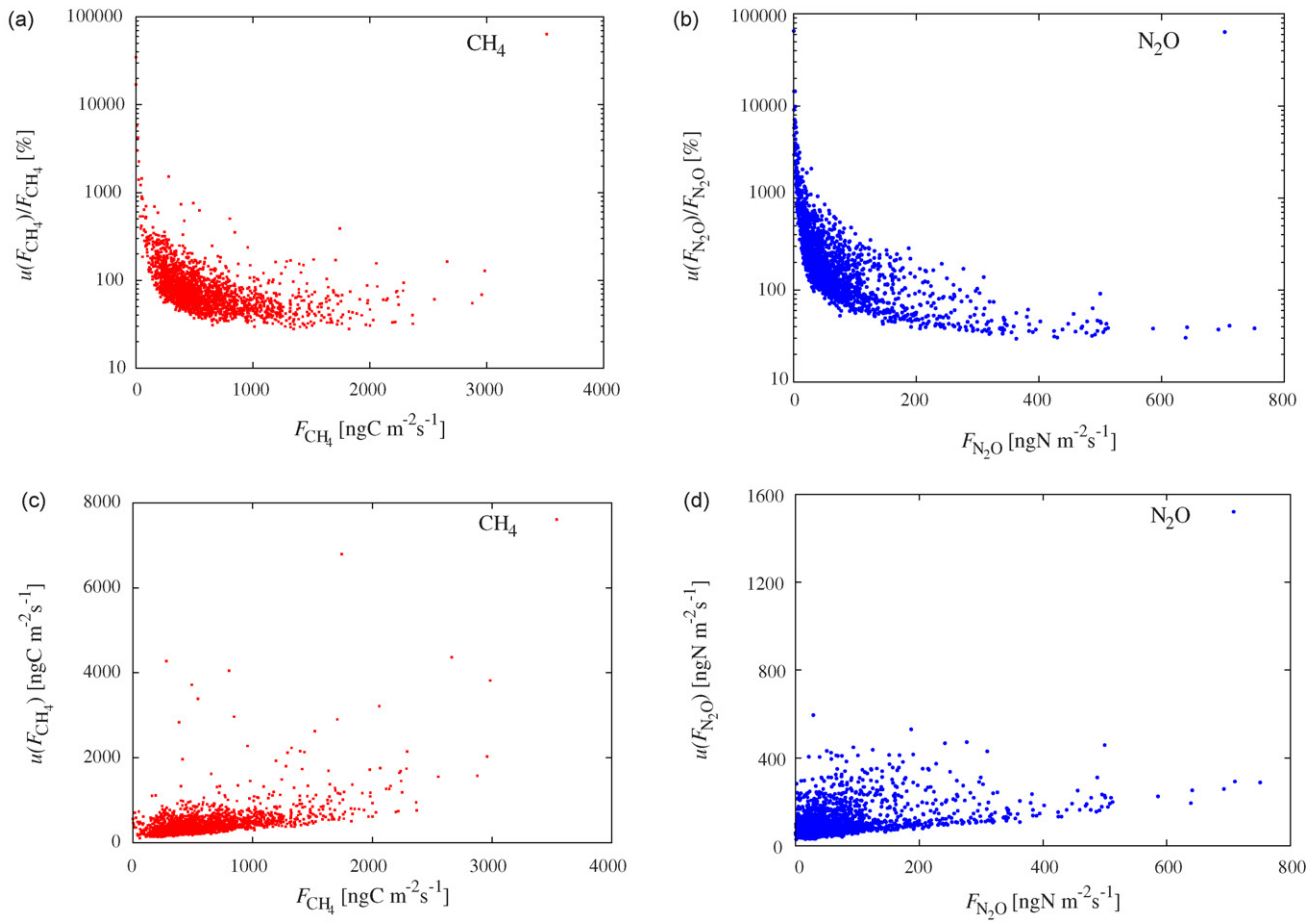

Fig. 5. Relative uncertainty of $N = 2185$ 30 min EC fluxes of CH_4 (a) and N_2O (b), and the absolute uncertainty of CH_4 (c) and N_2O (d) as function of the net ecosystem exchange of both gasses.

uncertainties are random. Therefore, we investigate the uncertainty in the EC flux over different time periods ranging from a single flux to a month. In that case, the uncertainty in the calibration correction algorithm decreases by $1/\sqrt{N_{session}}$ and all other uncertainties by $1/\sqrt{N}$, where $N_{session}$ denotes the number of calibration sessions. We select three flux magnitude ranges for both gasses and we calculate the 30 min uncertainty for each 30 min flux. Then, we assume 100% data coverage and we take each 30 min value for a daily or monthly value. Thus, we have the same number of 30 min, daily and monthly values, and they are also equal. Next, we determine the corresponding daily and monthly uncertainty for each value. Finally, we calculate the average 30 min, daily and monthly uncertainty within each flux magnitude range. We give an overview of the absolute and relative uncertainties in Tables 2 and 3 for CH_4 and N_2O, respectively.

The average uncertainty in a daily flux is smaller than 25% and 50% for CH_4 and N_2O, respectively, based on fluxes larger than 100 ng C m^{-2} s^{-1} and 15 ng N m^{-2} s^{-1}. This is quite promising since this implies that the annual uncertainty can even be below 10%. Uncertainty in annual flux estimates derived from chamber may be as high as 50% due to temporal and spatial variability in fluxes (Flechard et al., 2007). This means that EC flux measurements can contribute to more accurate estimates of net ecosystem exchange of both gasses than estimates only based on chamber measurements.

Table 2
Indication of absolute uncertainty in ng C m^{-2} s^{-1} and relative uncertainty in average CH_4 EC fluxes over different time periods. The data is selected from $N = 2185$ EC flux measurements. The average magnitude values are given together with their standard deviation and the average uncertainty together with their uncertainty range given by one standard deviation.

	Low fluxes	Normal fluxes	High fluxes
General information			
Selection range [ng C m^{-2} s^{-1}]	100–300	300–500	700–900
N in range	387	695	238
Average magnitude [ng C m^{-2} s^{-1}]	229 ± 48	400 ± 57	784 ± 55
Uncertainty			
30 min absolute [ng C m^{-2} s^{-1}]	322 (72–572)	360 (136–584)	520 (185–855)
30 min relative [%]	146 (42–250)	91 (37–145)	67 (25–109)
Daily absolute [ng C m^{-2} s^{-1}]	56 (20–92)	72 (36–108)	113 (52–176)
Daily relative [%]	25 (10–40)	18 (9–27)	14 (6–22)
Monthly absolute [ng C m^{-2} s^{-1}]	17 (8–26)	25 (11–39)	41 (12–70)
Monthly relative [%]	7 (3–11)	6 (3–9)	5 (1–9)

Table 3
Indication of absolute uncertainty in ng N m^{-2} s^{-1} and relative uncertainty in average N_2O EC fluxes over different time periods. The data is selected from $N = 2185$ EC flux measurements. The average magnitude values are given together with their standard deviation and the average uncertainty together with their uncertainty range given by one standard deviation.

	Low fluxes	Normal fluxes	High fluxes
General information			
Selection range [ng N m^{-2} s^{-1}]	15–35	40–60	90–110
N in range	556	366	117
Average magnitude [ng N m^{-2} s^{-1}]	25 ± 6	49 ± 6	99 ± 6
Uncertainty			
30 min absolute [ng N m^{-2} s^{-1}]	81 (32–130)	101 (44–158)	134 (55–213)
30 min relative [%]	342 (128–556)	208 (90–326)	136 (54–214)
Daily absolute [ng N m^{-2} s^{-1}]	12 (5–19)	15 (7–23)	21 (9–33)
Daily relative [%]	50 (19–81)	31 (14–48)	21 (9–33)
Monthly absolute [ng N m^{-2} s^{-1}]	2 (1–3)	3 (1–5)	5 (2–8)
Monthly relative [%]	10 (4–16)	7 (4–10)	5 (2–8)

5. Conclusion and discussion

An overview is given of the uncertainties in EC flux measurements of CH_4 and N_2O. The total EC flux uncertainty of a 30 min flux consists of several uncertainties either linked to the uncertainties in the correction algorithm of the systematic errors in EC flux measurements or linked to processes for which no corrections could be made. All uncertainties are random and decrease with increasing independent realizations. We split the uncertainties into four groups with different degree of randomness, per measurement point, per 30 min flux, per day and per calibration period. We assumed that the uncertainties with degree of randomness per measurement point are negligible in comparison to the other uncertainties.

Further, we estimated the relative and absolute uncertainty of a 30 min EC flux for CH_4 and N_2O for $N = 2185$ EC fluxes measured at a dairy farm site in the Netherlands. The average absolute uncertainty and its standard deviation in flux units were 500 ± 400 ng C m^{-2} s^{-1} for CH_4 and 100 ± 100 ng N m^{-2} s^{-1} for N_2O. The relative uncertainty distribution resembles a lognormal distribution, and the geometric average and standard deviation are 80% and 200% for CH_4, and 200% and 300% for N_2O, respectively. The corresponding 95% confidence intervals range from 20% to 300% for CH_4, and from 30% to 1800% for N_2O.The large relative uncertainties corresponded to relatively small EC fluxes.

The uncertainty was mainly caused by the uncertainty due to one-point sampling. On average this term contributed for more than 90% for both gasses on each 30 min EC flux uncertainty. The other 10% included the uncertainty in frequency response correction, Webb-correction and calibration correction. But, the uncertainty in rotation was not taken into account in this study; however, this uncertainty will also be much smaller than the one-point sampling uncertainty. EC averages over longer time spans than 30 min were needed to obtain more accurate emission estimates.

Therefore, we validated the effect of longer time spans on the uncertainty in the EC flux. We determined the 30 min, daily and monthly uncertainty for three flux magnitude ranges for both gasses. The average absolute uncertainties for CH_4 fluxes ranging from 300 to 500 ng C m^{-2} s^{-1} were 360, 72 and 25 ng C m^{-2} s^{-1} for 30 min, daily and monthly average, respectively, and the average absolute uncertainties for N_2O fluxes ranging from 40 to 60 ng N m^{-2} s^{-1} were 101, 15 and 3 ng N m^{-2} s^{-1}. Consequently, the average relative daily and monthly uncertainties were 18% and 6% for CH_4, and 31% and 7% for N_2O. These values indicate the uncertainty of the average EC flux value and not the uncertainty in the net ecosystem exchange. Then, the uncertainty in the storage change should be taken into account. In addition, the effect of an inadequate footprint, non-stationarity, advection and entrainment should be investigated as well.

In conclusion, the average uncertainty in a daily flux at field scale can be significantly smaller than 50% for both gasses which is quite promising. This means that EC flux measurements can seriously contribute to more accurate estimates of net ecosystem exchange of both gasses than estimates only based on chamber measurements.

Acknowledgements

This research was part of the Dutch National Research Program BSIK ME1. We are grateful to the anonymous referees for their critical remarks and suggestions. Thanks are due to our colleagues P. van den Bulk, P. Fonteijn and H. van 't Veen for their assistance during these measurements. We are also very grateful to E. Veenendaal of University of Wageningen for making available the latent heat flux data. Finally, we owe a special debt of gratitude to the farmer T. Van Eyk for using his farm site.

Appendix A

In this appendix, we derive an analytical expression for the "Businger"-factor $\varphi = \left(\overline{(w'c')^2} - \left(\overline{w'c'}\right)^2\right)/\left(\overline{w'c'}\right)^2$ for the case where w' and c' are given by a zero-mean joint-Gaussian stochastic process. The probability density function can then be described by three parameters, the standard deviations σ_w, $\boldsymbol{\sigma}_c$ and the correlation coefficient $\boldsymbol{\rho}_{wc}$ and is given by

$$P(w', c') = \frac{1}{2\pi\sigma_w\sigma_c\sqrt{1-\rho_{wc}^2}} \exp\left[-\frac{1}{1-\rho_{wc}^2}\left(\frac{w'^2}{2\sigma_w^2} + \frac{c'^2}{2\sigma_c^2} + \frac{\rho_{wc}w'c'}{\sigma_w\sigma_c}\right)\right] \tag{A.1}$$

By construction one has $\overline{w'^2} = \sigma_w^2$, $\overline{c'^2} = \sigma_c^2$ and $\overline{w'c'} = \sigma_w\sigma_c\rho_{wc}$; an expression for $\overline{(w'c')^2}$ can be found by evaluating the integral over $P(w', c')$, i.e.

$$\begin{aligned}\overline{(w'c')^2} &= \int\int (w'c')^2 P(w', c')dw'dc' = \sigma_w^2\sigma_c^2\left(1 + 2\rho_{wc}^2\right) \\ &= \overline{w'^2}\,\overline{c'^2} + 2\left(\overline{w'c'}\right)^2.\end{aligned} \tag{A.2}$$

Consequently, we obtain for $\boldsymbol{\varphi}$

$$\varphi = \frac{\overline{w'^2c'^2} + \left(\overline{w'c'}\right)^2}{\left(\overline{w'c'}\right)^2} = \frac{1}{\rho_{wc}^2} + 1 \tag{A.3}$$

Since $|\rho_{wc}| < 1$, this result shows that φ is bounded from below (the minimal value is $\varphi = 2$ at $\rho_{wc} = 1$), but not from above as φ diverges for $\rho_{wc} \to 0$. This leads us to conclude that there is no good justification for setting φ to a "universal" value, because even for an elementary Gaussian process φ can take any value larger than 2.

We emphasize that the problems with non-universal values of φ are rather pathological and an unnecessary result of expressing the uncertainty as a relative contribution. With hindsight it appears to be much wiser to stay close to the definition and treat the one-point sampling uncertainty as an absolute contribution described by

$$u_{\mathrm{op}} = \sqrt{\frac{20z}{T_{\mathrm{av}}U}}\sqrt{\overline{(w'c')^2} - \left(\overline{w'c'}\right)^2} \tag{A.4}$$

where we note that the second factor can be readily determined from the data.

References

Allan, D.W., 1966. Statistics of atomic frequency standards. Proceedings of the IEEE 54, 221–230.

Aubinet, M., Grelle, A., Ibrom, A., Rannik, Ü., Moncrieff, J., Foken, T., Kowalski, A.S., Martin, P.H., Berbigier, P., Bernhoffer, C., Clement, R., Elbers, J., Granier, A., Grünwald, T., Morgenstern, K., Pilegaard, K., Rebmann, C., Snijders, W., Valentini, R., Vesala, T., 2000. Estimates of the annual net carbon and water exchange of forests: the EUROFLUX methodology. Advances in Ecological Research 30, 113–175.

Bosveld, F.C., Beljaars, A.C.M., 2001. The impact of sampling rate on eddy-covariance flux estimates. Agricultural and Forest Meteorology 109, 39–45.

Businger, J.A., 1986. Evaluation of the accuracy with which dry deposition can be measured with current micrometeorological techniques. Journal of Climate and Applied Meteorology 25, 1100–1124.

De Roode, S.R., Duynkerke, P.G., Jonker, H.J.J., 2004. Large Eddy Simulation of the atmospheric boundary layers: how large is large enough? Journal of the Atmospheric Sciences 61, 403–421.

Eugster, W., Zeyer, K., Zeeman, M., Michna, P., Zingg, A., Buchmann, N., Emmenegger, L., 2007. Methodical study of nitrous oxide eddy co-variance measurements using quantum cascade laser spectrometry over a Swiss forest. Biogeosciences 4, 927–939.

Flechard, C.R., Ambus, P., Skiba, U., Rees, R.M., Hensen, A., Van Amstel, A., Van den Pol-van Dasselaar, A., Soussana, J.-F., Jones, M., Clifton-Brown, J., Raschi, A., Horvath, L., Neftel, A., Jocher, M., Ammann, C., Leifeld, J., Fuhrer, J., Calanca, P., Thalman, E., Pilegaard, K., Di Marco, C., Campbell, C., Nemitz, E., Hargreaves, K.J., Levy, P.E., Ball, B.C., Jones, S.K., Van de Bulk, W.C.M., Groot, T., Blom, M., Domingues, R., Kasper, G., Allard, V., Ceschia, E., Cellier, P., Laville, P., Henault, C., Bizouard, F., Abdalla, M., Williams, M., Baronti, S., Berretti, F., Grosz, B., 2007. Effects of climate and management intensity on nitrous oxide emissions in grassland systems across Europe. Agriculture, Ecosystems and Environment 121, 135–152.

Foken, T., Wichura, B., 1996. Tools for quality assessment of surface-based flux measurements. Agricultural and Forest Meteorology 78, 83–105.

Hargreaves, K.J., Fowler, D., Pitcairn, C.E.R., Aurela, M., 2001. Annual methane emission from Finnish mires estimated form eddy co-variance campaign measurements. Theoretical and Applied Climatology 70, 203–213.

Hendriks, D.M.D., Dolman, A.J., Van der Molen, M.K., Van Huissteden, J., 2008. A compact and stable eddy co-variance set-up for methane measurements using off-axis integrated cavity output spectroscopy. Atmospheric Chemistry and Physics 8, 1–13.

IPCC, 2001. Climate Change 2001: The Scientific Basis. Contribution of Working Group I to the Third Assessment Report of the Intergovernmental Panel on Climate Change. in: Houghton, J.T., Ding, Y., Griggs, D.J., Noguer, M., Van der Linden, P.J., Dai, X., Maskell,, K., Johnson, C.A. (eds). Cambridge University Press, Cambridge, United Kingdom and New York, NY, USA.

IPCC, 2006. Climate change 1995. Scientific and technical analyses of impacts, adaptations and mitigation. Contribution of Working Group II to the Second Assessment Report of the Intergovernmental Panel on Climate Change. Cambridge University Press, London, UK.

Jonker, H.J.J., Duynkerke, P.G., Cuijpers, J.W.M., 1999. Mesoscales fluctuations in scalars generated by boundary layer convection. Journal of the Atmospheric Sciences 56, 801–808.

Kaimal, J.C., Finnigan, J.J., 1994. Atmospheric Boundary Layer Flows, their Structure and Measurement. Oxford University Press.

Kaimal, J.C., Wyngaard, J.C., Izumi, Y., Coté, O.R., 1972. Spectral characteristics of surface-layer turbulence. Quarterly Journal of Royal Meteorological Society 98, 563–589.

Kormann, R., Meixner, F.X., 2001. An analytical footprint model for non-neutral stratification. Boundary-Layer Meteorology 99, 207–224.

Kroon, P.S., Hensen, A., Jonker, H.J.J., Zahniser, M.S., Van 't Veen, W.H., Vermeulen, A.T., 2007. Suitability of quantum cascade spectroscopy for CH_4 and N_2O eddy co-variance flux measurements. Biogeosciences 4, 715–728.

Kroon, P.S., Schuitmaker, A., Jonker, H.J.J., Tummers, M.J., Hensen, A., Bosveld, F.C., 2009. An evaluation by laser Doppler anemometry of the correction based on Kaimal co-spectra for high frequency losses of EC flux measurements of CH_4 and N_2O. Agric. Forest Meteorol, this issue, doi:10.1016/j.agrformet.2009.08.009.

Laville, P., Jambert, C., Cellier, P., Delmas, R., 1999. Nitrous oxide fluxes from a fertilized maize crop using micrometeorological and chamber methods. Agricultural and Forest Meteorology 96, 19–38.

Lee, X.L., Massman, W., Law, B., 2004. Handbook of Micrometeorology. Kluwer Academic Publishers, Dordrecht, The Netherlands.

McMillen, R.T., 1988. An eddy correlation technique with extended applicability to non-simple terrain. Boundary-Layer Meteorology 43, 231–245.

Moncrieff, J.B., Malhi, Y., Leuning, R., 1996. The propagation of errors in long-term measurements of land-atmosphere fluxes of carbon and water. Global Change Biology 2, 231–240.

Moore, C.J., 1986. Frequency response corrections for eddy correlation systems. Boundary-Layer Meteorology 37, 17–35.

Neftel, A., Flechard, C., Ammann, C., Conen, F., Emmenegger, L., Zeyer, K., 2007. Experimental assessment of N_2O background fluxes in grassland systems. Tellus 59B, 470–482.

Nelson, D.D., McManus, B., Urbanski, S., Herndon, S., Zahniser, M.S., 2004. High precision measurements of atmospheric nitrous oxide and methane using thermoelectrically cooled mid-infrared quantum cascade lasers and detectors. Spectrochimica Acta Part A 60, 3325–3335.

Nol, L., Verburg, P.H., Heuvelink, G.B.M., Molenaar, K., 2008. Effect of land cover data on nitrous oxide inventory in fen meadows. Journal of Environmental Quality 37, 1209–1219.

Smith, K.A., Clayton, H., Arah, J.R.M., Christensen, S., Ambus, P., Fowler, D., Hargreaves, K.J., Skiba, U., Harris, G.W., Wienhold, F.G., Klemedtsson, L., Galle, B., 1994. Micrometeorological and chamber methods for measurement of nitrous oxide fluxes between soils and the atmosphere: overview and conclusions. Journal of Geophysical Research 99, 16541–16548.

Stull, R.B., 1988. An Introduction to Boundary Layer Meteorology. Kluwer Academic Publishers.

Taylor, J.R., 1982. An Introduction to Error Analysis. University Science Books, California.

Van den Hurk, B.J.J.M., 1996. Sparse canopy parameterizations for meteorological models. Ph.D. Thesis. Wageningen University, The Netherlands.

Veenendaal, E.M., Kolle, O., Leffelaar, P., Schrier-Uijl, A.P., Van Huissteden, J., Van Walsem, J., Möller, F., Berendse, F., 2007. CO_2 exchange and carbon balance in two grassland sites on eutrophic drained soils. Biogeosciences 4, 1027–1040.

Webb, E.K., Pearman, G.I., Leuning, R., 1980. Correction of flux measurements for density effects due to heat and water vapour transfer. Quarterly Journal of Royal Meteorological Society 106, 85–100.

Werle, P., Kormann, R., 2001. Fast chemical sensor for eddy correlation measurements of methane emissions from rice paddy fields. Applied Optics 40, 846–858.

Wienhold, F.G., Frahm, H., Harris, G.W., 1994. Measurements of N_2O fluxes from fertilized grassland using a fast response tunable diode laser spectrometer. Journal of Geophysical Research 99 (16), 557–567.

Wyngaard, J.C., 1973. On surface layer turbulence. In: Hauge, D.A. (Ed.), Workshop on Micrometeorology. Am. Meteor. Soc., Boston, pp. 101–149.